Diffusion measurements with hydrogen and methane through reservoir rock samples

Julia Michelsen*, *Nils* Langanke, *Birger* Hagemann, *Sebastian* Hogeweg and *Leonhard* Ganzer

Clausthal University of Technology, Institute of Subsurface Energy Systems, 38678 Clausthal-Zellerfeld, Germany

Abstract. Since renewable energy sources are subject to intense fluctuations caused by changing weather conditions, storing energy in form of hydrogen in the underground is a promising way to maintain energy availability in the future. While storage in salt caverns is compensating short-term intermittency, the storage in porous reservoirs like depleted gas fields is more for the seasonal intermittency. For a safe storage operation, a fundamental knowledge about the mixing behaviour between hydrogen and the residual natural gas, primarily methane, which acts as a part of the cushion gas, is essential. Besides the pressure-driven advective and dispersive flux, molecular diffusion is an important process. For investigating molecular diffusion of hydrogen and methane in underground storage sites at reservoir conditions, diffusion measurements with reservoir rock samples were carried out by using a novel pseudo-stationary one-chamber method. The main component of the experimental setup is a core holder, which contains a large chamber at one side of the sample. Prior to the measurement, the chamber and the rock sample are filled with hydrogen. Then methane is injected at the opposite side of the chamber where a second gas line serves as outlet. The composition of the outflowing gas is analysed by a gas chromatograph. The effective diffusion coefficients, which were determined by comparing the measured data with a numerical simulation model, range between $5.00 \cdot 10^{-9}$ and $3.71 \cdot 10^{-7}$ m^2/s. Plotting of the effective diffusion coefficients versus pressure, temperature and water saturation show clear trends, which, however, are partly different than calculated by conventional correlations.

1 Introduction

In order to eliminate the use of fossil fuels stepwise, the share of renewable energy sources is steadily increasing. Storage solutions for energy are becoming more and more relevant. This is due to the fluctuating production of renewable energy sources caused by unstable weather conditions. Examples of such conditions include changing wind patterns and irregular sunlight. A promising way to balance the production and demand for ensuring a permanent availability of energy is the storage of excess energy in the form of hydrogen. In doing so, hydrogen works as an energy carrier and whenever energy is needed, hydrogen can be converted into electrical energy. One possibility to store hydrogen which became quite popular lately, is the storage of hydrogen in the underground. Suitable for an underground hydrogen storage are porous reservoirs like depleted natural gas fields or aquifers, or salt caverns [1]. While caverns are more intended to be used for the daily balance between energy production and consumption, porous storage sites are needed for the seasonal balance. In this study the focus is on depleted gas fields. It is necessary to get a fundamental understanding of the mixing behaviour of the injected hydrogen and the residual natural gas, mainly methane, in underground hydrogen storage (UHS). Natural gas which is still present in the underground works as part of the cushion gas to enable an efficient storage process. Knowledge about the mixing behaviour is important for making predictions of the performance of an underground storage site in the future. An overview of the predominant mixing effects in an UHS is presented in Fig.1.

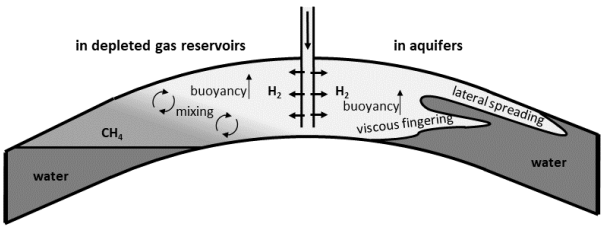

Fig. 1. Sketch of gas mixing effects in an UHS

The processes that is primarily causing and influencing the mixing process is hydrodynamic dispersion, which is a combination of molecular diffusion and mechanical dispersion [2, 3]. In this work an experimental method for the measurement of molecular diffusion in reservoir rocks is developed. Afterwards the method is applied to dry and partly water saturated reservoir rock samples from potential UHS sites in Europe. The rock type of the samples is mostly sandstone. In the past, diffusion measurements

* Corresponding author: julia.michelsen@tu-clausthal.de

have been carried out in several studies. However, these measurements were made with rocks, gases, and pressure and temperature conditions that do not correspond to those of potential UHS sites. For this reason, it is necessary that further diffusion measurements are carried out. Measurements of molecular diffusion with hydrogen and methane through storage rock samples were performed in this study. To investigate the impact of temperature, pressure and water saturation on the diffusion process, the measurements are done under various measurement conditions. The measurement results are used to determine effective diffusion coefficients, which can be later used in reservoir simulators for the prediction of future storage scenarios.

2 Fluid properties of hydrogen

The effectiveness and safety of UHS are significantly influenced by fluid properties of the stored gases. The injection of gas with high concentrations of hydrogen into a porous reservoir has an extensive impact on thermodynamic properties, affecting the volume and energy density of stored fluids. Moreover, it significantly influences the transportation process.

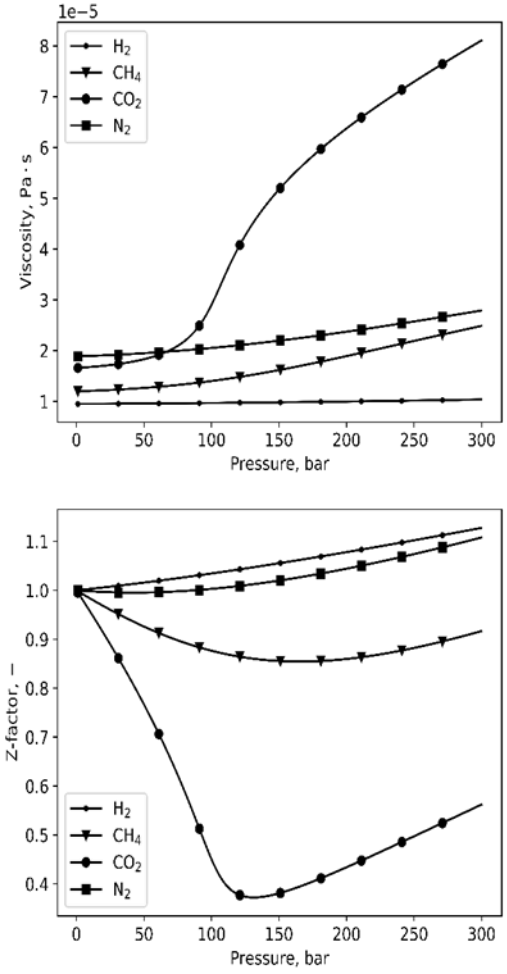

Fig. 2. Z-factor and viscosity versus pressure at a temperature of T=50°C; The compressibility is modelled based on the Peng and Robinson EoS [4], and the dynamic viscosity is based on a combination of the Stiel and Thodos and Lohrenz correlations [5, 6]

Hydrogen, being the lightest chemical element, exhibits low viscosity and less compressibility compared to most other gases. Fig. 2 provides an illustration of the relationship between compressibility (z-factor) and viscosity relative to pressure, in comparison to relevant natural gas components. While most gases have a z-factor below one at higher pressures, indicating increased compressibility, hydrogen's compressibility worsens as pressure increases. In terms of viscosity, hydrogen has the lowest values, roughly 1-1.5 times smaller than methane. The impact of density primarily affects phenomena such as gravity override, whereas viscosity could lead to unstable displacements characterized by viscous fingering. Furthermore, differences in interfacial tension, affecting relative permeability curves, can further modify the displacement process of the two phases.

The diffusion coefficient of hydrogen differs from other gases. This can be seen in the Stokes-Einstein equation [7]:

$$D = \frac{k_B T}{6\pi\eta r} \quad (1)$$

where D is the diffusion coefficient, k_B is the Boltzmann constant, T the absolute temperature, η the dynamic viscosity and r the radius of the spherical particle.

Here, the viscosity is in the denominator. Since hydrogen has a low viscosity, the resulting diffusion coefficient is smaller than for gases with a higher viscosity. In addition, the smaller molecular size of hydrogen contributes to a higher diffusivity.

3 Gas mixing in porous reservoirs

Understanding the way gases mix in porous reservoirs is decisive for the functioning of underground storage sites. Knowledge of the mixing behaviour is especially important for assessing the ability to recover stored hydrogen from the porous reservoir. There are two primary mechanisms responsible for the mixing of miscible gases. Firstly, advective flow plays a role, which is influenced by factors such as gravity, viscosity, capillarity, and compressibility. Secondly, gas mixing occurs through diffusive and dispersive processes [8]. Mechanical dispersion is a mixing process of fluids due to their movement and current in porous media. It can be divided into transversal and longitudinal dispersion. Transversal dispersion involves the spreading of fluid components perpendicular to the main flow direction, while longitudinal dispersion refers to the spreading along the main flow direction. Dispersion is driven by variations in the flow velocity which can occur on different scales. Fig. 3 illustrates the connection between molecular diffusion and mechanical dispersion in porous media and its relation to the flow velocity. In a gas storage the flow velocity varies over time depending on whether gas is being injected or produced. Moreover, the flow velocity depends on the location since the velocity is much higher near the wellbore than further away. Furthermore, the flow velocity depends on the permeability of the layer, as the flow velocity is greater in

layers with high permeability than in areas with a low permeability. When the flow velocity is low, molecular diffusion primarily governs the mixing process. On the other hand, higher velocities result in a transport that is primarily controlled by mechanical dispersion. The transitional region between these two extremes is influenced by both processes simultaneously [9].

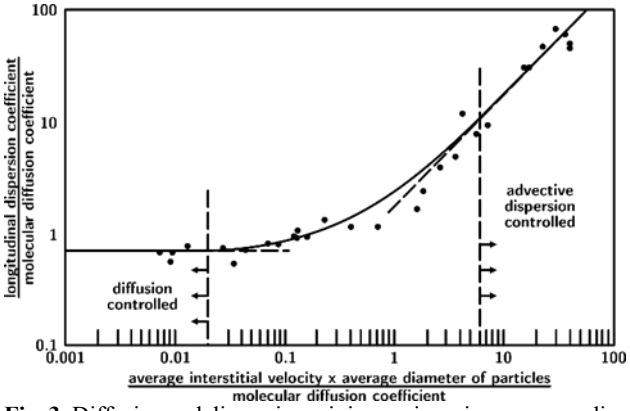

Fig. 3. Diffusive and dispersive mixing regimes in porous media flow (adapted from [9])

4 Molecular diffusion of hydrogen in the gas phase

Molecular diffusion is a physical process that is driven by chemical potential and occurs without pressure differences. The process refers to the movement of molecules driven by the inherent tendency to equalize concentration gradients, which arises from the random motion known as Brownian motion. It can take place under both stationary and unsteady conditions. The difference between the two conditions is that stationary diffusion occurs at a constant rate, while the unsteady diffusion rate is a function of time. Both types of diffusion can be explained using Fick's laws and can be utilized to determine the diffusion coefficient. According to Fick's first law, the diffusion flux is directly proportional to the gradient in concentration [10].

The diffusivity in a porous medium is typically lower compared to free diffusion of gases, as the gas encounters less space and must traverse a greater distance within the porous medium. Various factors, such a porosity, tortuosity, and the existence of other fluid phases within the pores, influence the effective diffusivity. In the case of binary systems, the diffusive flux of gas components in a porous medium can be represented by the following equation:

$$J^k_{\text{diff}} = -\rho D^{AB}_{eff} \nabla c^k \tag{2}$$

In the given equation, J^k_{diff} represents the flux of component k resulting from diffusion, measured in mol/m²/s, ρ denotes the molar density of the gas in mol/m³, while D_{eff} represents the effective diffusion coefficient for the binary system, measured in m²/s. ∇c^k is the gradient of the mole fraction for component k.

By combining equations by Fuller [11, 12, 13] and Millington & Quirk [14] the effective diffusion coefficient can be expressed as follows:

$$D^{AB}_{eff} = \phi S_g \tau D^{AB}_{bulk}(p,T) \tag{3}$$

where ϕ is the porosity, S_g the gas saturation, τ the tortuosity factor and D^{AB}_{bulk} the bulk diffusion coefficient in m²/s.

For the description of diffusion in porous media the tortuosity of the pore structure needs to be considered. The model of Millington & Quirk estimates the tortuosity factor of a porous medium based on its porosity and gas saturation:

$$\tau = \phi^{1/3} S_g^{7/3} \tag{4}$$

Knudsen diffusion occurs when the average distance covered by gas molecules, known as the mean free path, becomes comparable to or larger than the pore sizes of the porous medium. Consequently, the molecules collide more frequently with the walls of the pores rather than with each other. The extent of Knudsen diffusion can be quantified by the Knudsen number, denoted as K_n. A Knudsen number greater than 10 indicates the dominance of Knudsen diffusion, where collisions between molecules and the pore walls are the primary factor. To determine whether Knudsen diffusion is a factor in the experiments conducted within this study, the Knudsen number is calculated using the equation provided by Bear (2018) [15]:

$$K_n = \frac{\lambda}{l_{pm}} \tag{5}$$

λ represents the mean free path of molecules in meters, while l_{pm}denotes the characteristic length dimension of the void space, specifically the pore diameter, also in meters. In the case of the measurements conducted using Bentheimer sandstone, one of the samples used, assuming a mean free path of $6.6 \cdot 10^{-8}$ m and a mean pore diameter of $5 \cdot 10^{-5}$ m, the calculated Knudsen number is $1.32 \cdot 10^{-3}$. Therefore, it can be concluded that Knudsen diffusion does not have a significant influence on the measurements performed in this particular case.

4.1 Molecular diffusion measurements in literature

Numerous devices and techniques have been devised to measure effective molecular diffusion within porous materials. One of these techniques is the Wicke-Kallenbach method, which operates under steady-state conditions and has been described by Ho and Webb (2006) [16] and Soukup et al. (2008) [17]. This approach involves employing a diffusion cell comprising two chambers separated by a porous sample. The measurement utilizes two gases, each flowing continuously through its respective chamber. The pressure within both chambers is maintained at a constant level throughout the experiment. Gas chromatography is employed to continuously analyse the

gas compositions within both chambers. The measurement procedure assumes that there is no flow in the porous membrane. The flow exists only in the chambers, but is very slow, so that no flow is assumed in the pore space.

The Graham cell is an alternative technique for measuring diffusion, which shares similarities with the Wicke-Kallenbach method, as described by Soukup et al. (2008).

In the Graham cell method, two gases flow continuously through separate chambers and the porous medium until a steady diffusion state is achieved. Subsequently, the inflow and outflow on one side are closed, allowing for the determination of the diffusive volume flow using a flow meter Unlike the Wicke-Kallenbach method, continuous analysis and monitoring of the outflowing gas from both chambers are not required in the Graham cell method.

An overview of diffusion measurements reported in the literature, along with their corresponding results, is provided in Table 1.

Chen et al. (1977) [18] conducted diffusion experiments using modified Wicke-Kallenbach setups on porous samples. In their experiments the binary diffusion of methane and nitrogen through sandstone samples was measured and effective diffusion coefficients were determined. The resulting effective molecular diffusion coefficients vary between $2.59 \cdot 10^{-7}$ and $2.00 \cdot 10^{-5}$ for dry rock samples.

A similar approach was used by Pandey et al. (1974) [19] for the diffusion measurement of helium and nitrogen through porous rock samples. The diffusion was measured at steady state but also at unsteady state conditions. At steady state conditions, the diffusion coefficients lie between $2.14 \cdot 10^{-8}$ to $1.19 \cdot 10^{-6}$ m^2/s for dry rock samples. The diffusion coefficients at unsteady state conditions are between $1.67 \cdot 10^{-10}$ to $1.88 \cdot 10^{-7}$ m^2/s.

Guevara-Carrion et al. (2019) [20] examined the diffusion of methane in supercritical carbon dioxide under elevated pressure, but without a porous medium. In this work a Taylor dispersion apparatus was used. The measured effective molecular diffusion coefficients show a range from $1.46 \cdot 10^{-8}$ to $3.70 \cdot 10^{-8}$ m^2/s.

Strauch et al. (2023) [21] investigated the diffusion of hydrogen through different potential storage site rocks. In their study sandstone, rock salt and claystone samples were used. An experimental set-up, which comprises two chambers and a rock sample, was developed to determine hydrogen breakthrough times and hydrogen diffusion coefficients. The determined effective diffusion coefficients in these experiments range from 10^{-9} to 10^{-8} m^2/s. It has been observed that water decreases the velocity of diffusion in all conducted experiments.

In the study by Arekhov et al. (2023) [22] an experimental setup was constructed, which enables the measurement of effective multicomponent diffusion coefficients at high pressure and temperature conditions. For the diffusion measurements three different reservoir rocks of a potential UHS storage site were used. The determined diffusion coefficients vary between $1.49 \cdot 10^{-7}$ and $1.51 \cdot 10^{-6}$ m^2/s.

It can be concluded that the diffusion coefficients determined in the literature show a range which is too large for the use of these values for future applications. In addition, there are only a few diffusion experiments in literature, where hydrogen was used. For UHS it is necessary to conduct diffusion experiments with hydrogen under reservoir conditions (pressure and temperature) and to use appropriate storage rock samples.

5 Method and experimental procedure

The measurement of effective diffusion was performed for binary gas systems. For the measurement a pseudo-stationary one-chamber measurement method was developed. The main component of the experimental setup is a core holder, which is designed for rock samples with a length of up to 6 cm and a diameter of 3 cm, as shown in Fig. 5.

The rock sample, a hollow cylinder, a gas distribution element, a gas injection element and two end pieces are installed into the core holder, which is also called diffusion cell.

Table 1. Molecular diffusion experiments in literature

Reference	Gases	Temperature [°C]	Pressure [bar]	Method	Material	Effective diffusion coefficient [m^2/s]
Pandey et al. (1974)	He, N_2	24 - 42	1 - 5	Steady state flow (for dry samples), unsteady-state flow (for low permeability and water-saturated samples)	Carbonate, sandstone and shale samples	Steady state: $2.14 \cdot 10^{-6}$ to $1.19 \cdot 10^{-4}$ Unsteady state: $1.67 \cdot 10^{-8}$ to $1.88 \cdot 10^{-5}$ (only dry samples considered)
Chen et al. (1977)	CH_4, N_2	35	1	Steady state flow (modified Wicke-Kallenbach)	Sandstone samples	$2.59 \cdot 10^{-7}$ to $2.00 \cdot 10^{-5}$ (only dry samples considered)
Guevara-Carrion et al. (2019)	CH_4, CO_2	19.4 – 59.7	90 - 147	Taylor set-up	Bulk	$1.46 \cdot 10^{-8}$ to $3.70 \cdot 10^{-8}$
Strauch et al. (2023)	H_2	Room temperature	1	Unsteady state	Sandstone, claystone, rock salt-samples	10^{-9} to 10^{-8}
Arekhov et al. (2023)	H_2, CH_4	28	5 - 40	Unsteady state	Sandstone samples	$8.38 \cdot 10^{-7}$ to $1.51 \cdot 10^{-6}$

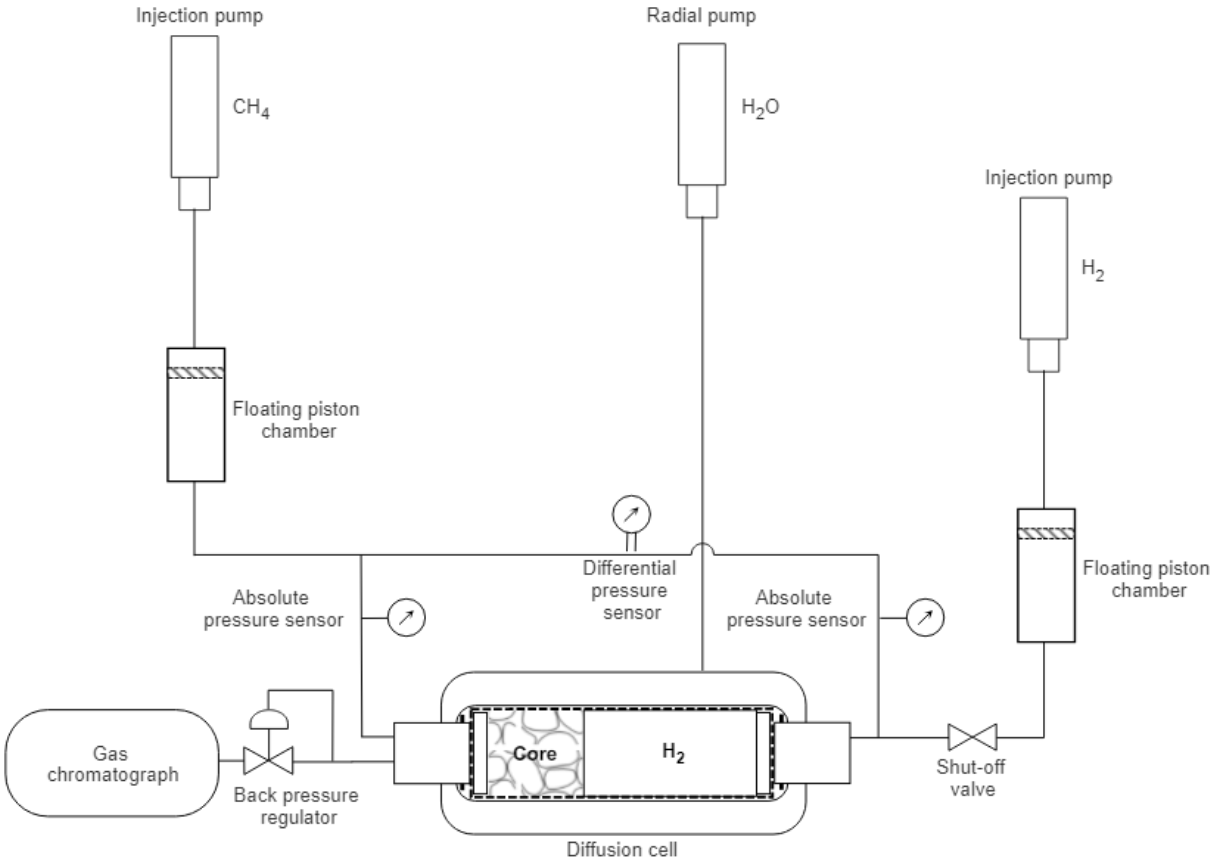

Fig. 5. Simplified sketch of the experimental setup

The hollow cylinder is the so called "chamber" of this measurement method. There is a second chamber, which is in the grooves of the gas distribution element having an extremely small volume. Before installing these components into the diffusion cell, they are pushed into a Viton sleeve. The diffusion cell is then pressurized by water with a radial pressure, which must be higher than the measuring pressure of the gases. The hollow cylinder is located at one side of the rock sample. It must have a volume multiple times larger than the pore volume of the rock sample. This chamber has one inlet. Prior to the measurement the chamber is filled with hydrogen gas at the desired pressure. On the other side of the sample is the gas distribution element, which has one inlet and one outlet. During the experiment methane is injected into the cell via this inlet. The injection is controlled by a syringe pump, which drives a floating piston chamber. At the outlet of the gas distribution element a backpressure regulator is installed, which regulates the pressure in the diffusion cell to a constant value during the measurement. Behind the backpressure regulator a gas chromatograph repeatedly analyses the composition of the outflowing gas. A simplified sketch of the experimental setup is shown in Fig.5.

The measurement of molecular diffusion coefficients is done by the following steps:

Sample installation: The core sample is pushed into a Viton sleeve together with the chamber, the target and the two end pieces. The components are installed into the core holder. The core holder is connected to the experimental setup.

Leakage test: Radial and system pressure are built up stepwise to reduce and minimize stresses in the core sample. The radial pressure must be 1.5 times (or 50 bar) higher than the injection pressure. A leakage test with nitrogen is performed, during which the leakage rate should not exceed 0.5 % of the injection rate in the experiment.

Preparation: The chamber and the core sample are flooded with hydrogen. The purity of the outflowing gas is repeatedly analyzed by the gas chromatograph until a gas purity of 99.9 % hydrogen is reached. The chamber is pressurized. The increasing of the pressure is done by using a gas booster. The floating piston chamber is filled with methane. Here, again a gas purity of 99.9 % must be ensured. This is achieved by repeated flushing of the floating piston chamber. Pressurizing the floating piston chamber is done with the gas booster.

Measurement: The injection of methane is started at a constant rate. The shut-off valve separating the core holder and the floating piston chamber is opened. The composition of the outflowing gas is analyzed with the gas chromatograph every three minutes.

6 Core samples

The diffusion measurements were performed with core material from potential UHS sites. A total of seven rock samples from the core material provided by industry partners were chosen.

Table 2. Rock samples for the diffusion measurements and their properties

Sample site/formation	Rock type	Porosity [%]	Permeability [mD]	Site conditions	
				Mean pressure [bar]	Temperature [°C]
Bentheimer sandstone	Sandstone	24.7	2500.0	-	-
Berea sandstone	Sandstone	21.0	105.0	-	-
Chattian Sand	Sandstone	29.9	71.0	106.0	50.0
Aquitanian formation	Sandstone	26.8	157.6	53.5	25.0
Pliocene Sands	Sandstone	31.7	718.6	88.3	45.0
Ebes Fm.	Limestone	19.9	23.6	140.5	107.0
Ujfalu Fm. 1	Sandstone	32.1	288.2	116.5	86.0
Detfurth formation	Sandstone	27.4	263.1	287.2	96.0
Rough Rotliegendes	Sandstone	17.6	17.2	203.0	92.0

The samples are mainly sandstone. Additionally, a Berea sandstone sample, and a Bentheimer sandstone reference sample were selected from a surface quarry. Table 2 provides a comprehensive list of all the samples used, along with their respective properties

The samples show a broad range in permeability and porosity. The porosity of the samples was determined using a gas pycnometer (micromeritics AccuPyc II 1340) with helium as the measuring medium. Permeability measurements were performed on a core flooding cell using nitrogen. The radial pressure applied during the permeability measurements was 20 bar, while the gas pressure was approximately 10 bar. The "mean pressure" was defined as the arithmetic mean between the minimum and maximum allowable operating pressure at the reference depth (e.g., the midpoint of the reservoir). Alternatively, for locations that have not been used for gas storage previously, the mean pressure is defined as $0.75 \cdot p_{\text{init}}$.(initial reservoir pressure).

7 Interpretation and calculation of effective diffusion coefficients

The experimental results were interpreted by using a one-dimensional numerical simulation model. This was used to obtain the effective diffusion coefficient by a model fitting process. The numerical simulation model was implemented in COMSOL Multiphysics. The model solves the following partial differential equation, which is based on Fick's second law, in a one-dimensional domain:

$$\frac{p}{RT}\phi\frac{\partial c}{\partial t} = \frac{p}{RT}D\frac{\partial^2 c}{\partial x^2} \tag{6}$$

where p is the measurement pressure in Pa, R is the universal gas constant in J/(mol*K), T is the measurement temperature in K, ϕ is the porosity of the sample, c is the molar fraction of hydrogen and D is the effective diffusion coefficient in m²/s.

The following differential equations describe the boundary conditions. On the left side, no hydrogen is injected, but hydrogen which is transported into the groove of the target by diffusion flows out:

$$\frac{pV_l}{RT}\frac{\partial c_l}{\partial t} = -qc_l + \frac{p}{RT}DA\nabla c_1 \tag{7}$$

where V_l is the volume of the left chamber in m³, q is the injection rate in mol/s, A is the end face of the rock sample, ∇c_1 is the space derivative of the hydrogen concentration at position 1, c_l is the hydrogen concentration in the left chamber. On the right side, a similar differential equation is solved:

$$\frac{pV_r}{RT}\frac{\partial c_r}{\partial t} = -\frac{p}{RT}DA\nabla c_2 \tag{8}$$

where V_r is the volume of the right chamber in m³, ∇c_2 is the spatial derivative of the hydrogen concentration at position 2 and c_r the hydrogen concentration in the right chamber.

The matching of the simulation with the measurement is done by hand. As an example, Fig. 6 shows a comparison of a laboratory measurement with the simulation model. This measurement was done at 125 bar and 40 °C. The determined effective diffusion coefficient is $1.25 \cdot 10^{-7}$ m²/s. For determining the uncertainty of the matching process simulation results with effective diffusion coefficients with deviations of ±5 % are added to the plot. It can be recognized that the uncertainty is much smaller than 5%. It is estimated to be between 1 and 2%.

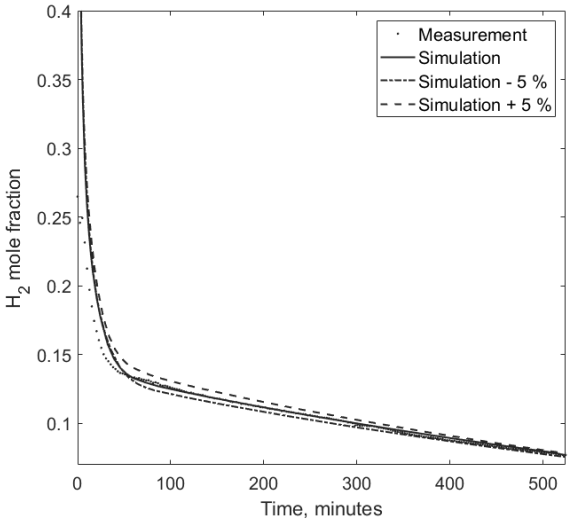

Fig. 6. Comparison of the simulation with the measurements

8 Validation and error estimation

A similar approach for the measurement of effective molecular diffusion of hydrogen in reservoir rocks was done by Arekhov et. al [22]. There and in this study, a measurement with a Berea sandstone sample was conducted. The measurement conditions were 60 bar and 25/28 °C. The measurement in this work led to an effective diffusion coefficient of $1.15 \cdot 10^{-7}$ m²/s. Arekhov et. al determined an effective diffusion coefficient of $2.09 \cdot 10^{-7}$ m²/s. Both measurements are in the same order of magnitude. While the porosity of the samples is similar, the deviation could be related to the different permeabilities of the samples. Arekhov et. al measured a permeability of 277 mD, whereas the permeability in this study was determined as 105 mD. Possibly the higher permeability results in a slightly higher effective diffusion coefficient.

An estimation of the potential error occurring during the measuring procedure was done. Here, the main factors that might cause uncertainties are related to pressure, temperature and measured gas concentration. The error estimation takes into account the random and the systematic error.

First, the random error of the measurement method was estimated. This was done by conducting the measurement with the Bentheimer sandstone sample at reference conditions (100 bar, 40 °C) three times. A mean value of the measurements was calculated based on the following equation [23]:

$$\bar{x} = \frac{\sum_{i=1}^{N} x_i}{N} \tag{9}$$

where N is the number of measurements and x_i are the results of the measurements. The results for effective diffusion coefficients of the measurements are $1.10 \cdot 10^{-7}$, $1.20 \cdot 10^{-7}$ and $1.25 \cdot 10^{-7}$ m²/s. The mean value is $1.18 \cdot 10^{-7}$ m²/s.

The standard deviation is calculated using the following equation:

$$\sigma = \sqrt{\frac{1}{N-1}\sum_{i=1}^{N}(x_i - \bar{x})^2} \tag{10}$$

The standard deviation for these measurements is $5.56 \cdot 10^{-9}$ m²/s.

For the estimation of the systematic error the uncertainties of the pressure, temperature and measurement of the gas concentration were estimated and combined by using the following equation for the calculation of error propagation:

$$\delta D(p,T,c) = \sqrt{(\delta p \frac{\delta D}{\delta p})^2 + (\delta T \frac{\delta D}{\delta T})^2 + (\delta c \frac{\delta D}{\delta c})^2} \tag{11}$$

where δD is the uncertainty of the effective diffusion coefficient, δp the uncertainty of the pressure, δT the uncertainty of temperature and δc the uncertainty of the measured gas concentration. The determined systematic error is $1.4 \cdot 10^{-9}$ m²/s.

The uncertainty for the pressure was determined by calculating the mean pressure value of all diffusion measurements at 100 °C and based on this, standard deviation from the desired measurement pressure (100bar) was calculated. The outcome was combined with the accuracy of the pressure sensor (0.018bar). For the uncertainty of the temperature, the error of the temperature sensor (0.23°C) and the estimated temperature fluctuations (0.2°C) were combined. The uncertainty of the measured gas concentration was determined by conducting 100 measurements with the gas chromatograph of a gas with a known composition (calibration gas) and calculating the standard deviation to the known value The derivatives of the effective diffusion coefficient according to the influencing factors were determined numerically. For pressure and temperature this was done by using the model of Fuller and Millington & Quirk (Equation 3, 4, 12 and 13) and for the measured gas concentration the simulation model (Equation 6 to 8) was used.

The overall uncertainty, which is a combination of the random and the systematic error is $5.73 \cdot 10^{-9}$ m²/s.

9 Results

As reference conditions for the diffusion measurements a pressure of 100 bar and a temperature of 40 °C was chosen. All samples were measured at these conditions. In addition, every sample was measured at the respective site conditions (cf. Table 2). The Bentheimer sandstone sample was used to investigate the influence of pressure, temperature and water saturation on diffusion. With this sample, measurements with a constant pressure of 100 bar and changing temperature as well as measurements with a constant temperature of 40 °C and various pressures were performed. Additionally, two measurements with a partly water-saturated Bentheimer sample (40 and 60 % water saturation) were done. Altogether, 36 diffusion measurements were performed covering a pressure range of 10 to

287.5 bar and a temperature range of 25 to 107 °C. For all measurements the effective diffusion coefficients were determined. The results of the measurements at the specific site conditions are summarized in Table 3.

Table 3. Effective diffusion coefficients determined based on the measurements

No.	Sample site/ formation	Rock type	P [bar]	T [°C]	Effective diffusion coefficient [m²/s]
1	Berea sandstone	Sandstone	40.0	25.0	$1.15 \cdot 10^{-7}$
1	Berea sandstone	Sandstone	60.0	25.0	$6.50 \cdot 10^{-8}$
2	Chattian Sand	Sandstone	106.0	50.0	$6.50 \cdot 10^{-8}$
3	Aquitanian formation	Sandstone	53.5	25.0	$1.10 \cdot 10^{-7}$
4	Pliocene Sands	Sandstone	88.3	45.0	$2.00 \cdot 10^{-7}$
5	Ebes Fm.	Limestone	140.5	107.0	$1.70 \cdot 10^{-8}$
6	Ujfalu Fm. 1	Sandstone	116.5	86.0	$1.10 \cdot 10^{-7}$
7	Detfurth formation	Sandstone	287.2	96.0	$1.70 \cdot 10^{-7}$
8	Rough Rotliegendes	Sandstone	203.0	92.0	$9.00 \cdot 10^{-9}$

The measurement results for the nine samples at the reference conditions (100 bar, 40 °C) are shown in Fig. 7. The numbers from Table 3 act as a key to identify the samples. The Bentheimer sandstone sample was added (9).

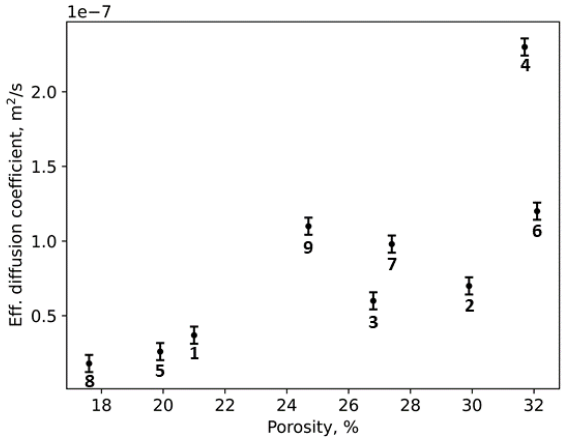

Fig. 7. Effective diffusion coefficient vs. porosity for all rock samples at 100 bar and 40 °C. Error bars represent standard deviation.

Here, the determined effective molecular diffusion coefficients are plotted against the porosity of the corresponding sample. There is a clear trend, that the effective diffusion coefficient increases with an increasing porosity.

The behaviour of the effective diffusion coefficient in dependence of pressure, temperature and water saturation measured with the Bentheimer sandstone sample is shown in Fig.8 to Fig. 10.

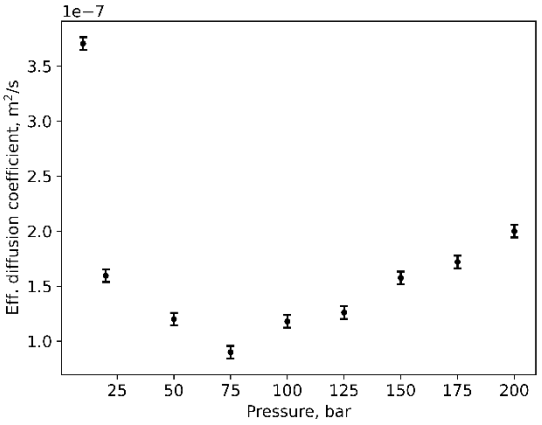

Fig. 8. Effective diffusion coefficient vs. pressure for the Bentheimer sandstone sample at 40 °C. Error bars represent standard deviation.

At a low pressure a decreasing trend in the effective diffusion coefficient can be observed with rising pressure. From 75 to 200 bar the trend is contrary. In this range, the diffusion coefficient is increasing with increasing pressure.

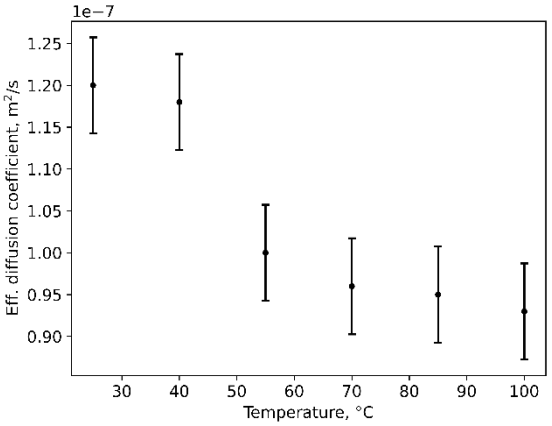

Fig. 9. Effective diffusion coefficient vs. temperature for the Bentheimer sandstone sample at 100 bar. Error bars represent standard deviation.

At measurements with a constant pressure of 100 bar and changing temperatures from 25 to 100 °C the effective diffusion coefficient shows a decreasing trend with increasing temperature.

As water saturation increases, there is a clear decrease in the effective diffusion coefficient, with the dry core sample having the highest effective diffusion coefficient of $1.10 \cdot 10^{-7}$ m²/s, the sample with 40 % water saturation having $4.00 \cdot 10^{-8}$ m²/s, and the 60 % water saturation sample having $5.00 \cdot 10^{-9}$ m²/s.

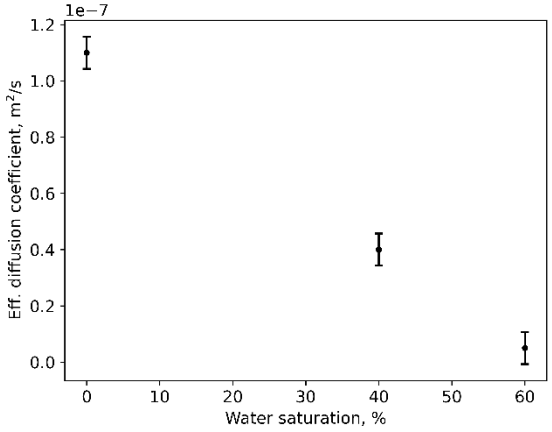

Fig. 10. Effective diffusion coefficient vs. water saturation at 100 bar and 40 °C. Error bars represent standard deviation.

10 Discussion

The following equation (6) for the description of the bulk binary diffusion coefficient D_{bulk}^{AB} is based on the model by Fuller [16, 17, 18]. This correlation enables the predication of diffusion coefficients for different combinations of components.

$$D_{bulk}^{AB}(p,T) = \frac{0.0143T^{1.75}}{pM_{AB}^{0.5}((\sum v)_A^{1/3}+(\sum v)_B^{1/3})^2} \quad (12)$$

$$M_{AB} = \frac{2}{\frac{1}{M_A}+\frac{1}{M_{AB}}} \quad (13)$$

where D_{bulk}^{AB} is the bulk binary diffusion coefficient in m^2/s, T is the temperature in K, p is the pressure in Pa, M_{AB} is the harmonic mean of the molecular weight of components A and B in g/mol, and $\sum_v$ is the atomic diffusion volume.

According to the equations, it can be inferred that the effective diffusion coefficient is inversely proportional to pressure. This relationship is evident from the data points from 10 to 75 bar. However, for higher pressures, the measurements exhibit a different pattern. Specifically, from 75 to 200 bar, there is a noticeable increasing trend. A comparable relationship between the diffusion coefficient and pressure was observed in a study conducted by Guevara-Carrion et al. (2019) for the binary system consisting of methane and carbon dioxide. A comparison of the experimental results with the Bentheimer sandstone sample and a model, which is a combination of Fuller and Millington & Quirk, is shown in Fig. 11. The measured and correlated values are in the same order of magnitude. The trend of the experimental data and the correlation is similar until 75 bar, although the values are not the same. For the measurements from 75 to 200 bar the correlation does not display the trend of the measurements since the experimental values are increasing but the correlated values are decreasing. The deviation from conventional correlations in this pressure region could be related to the supercritical state where drastic changes of the thermodynamic properties could take place along certain pathways across the Widom line.

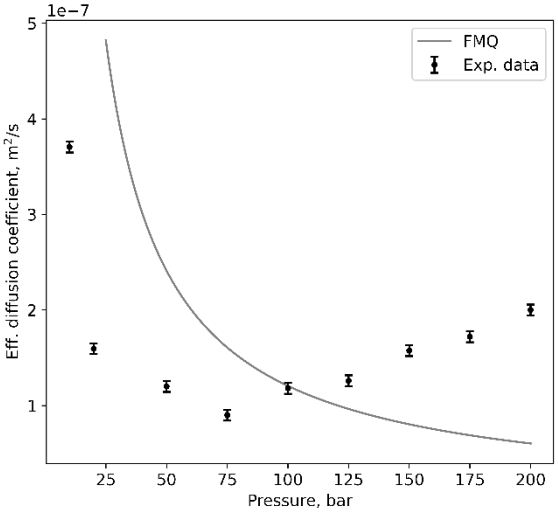

Fig. 11. Comparison of correlated (model Fuller and Millington & Quirk) and measured effective diffusion coefficient (Bentheimer sandstone sample, 40 °C). Error bars represent standard deviation.

The comparison of the experimental data of the measurements with the Bentheimer sandstone sample at varying temperatures with the correlated results of the model by Fuller and Millington & Quirk is depicted in Fig. 12 (constant pressure of 100 bar).

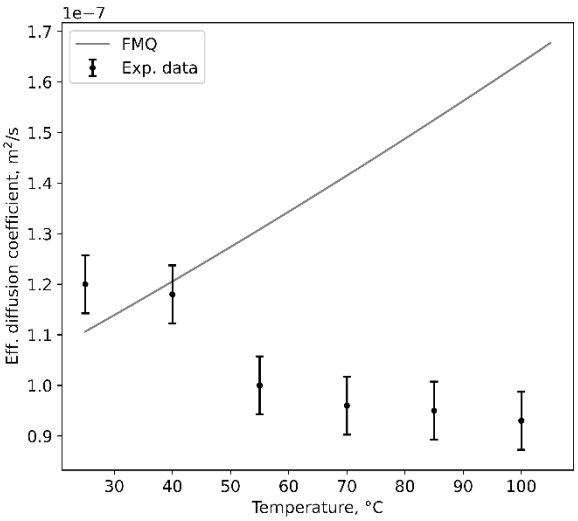

Fig. 12. Comparison of correlated (model Fuller and Millington & Quirk) and measured effective diffusion coefficient (Bentheimer sandstone sample, 100 bar). Error bars represent standard deviation.

The trend of the effective diffusion coefficient in the correlation is contrary to the trend observed in the laboratory but the measured effective diffusion coefficients are in the same order of magnitude. At 100 °C, when the experimental result and the correlation are furthest apart, the correlated result is approximately 1.8 times larger than the

experimentally determined diffusion coefficient. The unexpected decrease with rising temperature in the experimental measurements was also observed by Guevara-Carrion et al. (2019) in specific pathways within the supercritical region.

For the measurements with different water saturations, there is a clear decreasing pattern observed in the effective diffusion coefficient. The dry core sample has an effective diffusion coefficient of $1.10 \cdot 10^{-7}$ m^2/s, while at 40 % water saturation, it decreases to $4.00 \cdot 10^{-8}$ m^2/s, and at 60 % water saturation, it further reduces to $5.00 \cdot 10^{-9}$ m^2/s. This behaviour aligns with expectations, as higher water saturation results in reduced pore space for gas diffusion within the rock sample. These findings are consistent with the correlation proposed by Millington and Quirk.

11 Conclusion

In this study a new experimental setup was developed for the measurement of hydrogen diffusion through reservoir rocks. The measurement method that was used is a pseudo-stationary one chamber method. Based on the measured diffusion rates, effective diffusion coefficients were determined by comparing the measured data with a numerical simulation model. The measurements are repeatable, and the results are comparable to results from other diffusion measurements from literature. The plotting of the effective diffusion coefficients versus pressure, temperature and water saturation show clear trends, which, however, are partly different than calculated by conventional correlations. The measurements indicate deviations from the correlations at pressures above 75 bar, where the effective diffusion coefficient increases with increasing pressure. The temperature dependence is also not reflected by the correlation. The decreasing trend of the effective diffusion coefficient with increasing water saturation fits to the expectation. For a better understanding of the influence of temperature and pressure on the diffusion process, more measurements should be performed to get further data points.

This project has received funding from the Fuel Cells and Hydrogen 2 Joint Undertaking (now Clean Hydrogen Partnership) under grant agreement No 101006632. This Joint Undertaking receives support from the European Union's Horizon 2020 research and innovation programme, Hydrogen Europe and Hydrogen Europe Research. Additionally, we would like to thank TÜV Nord AG/DMT GmbH & Co. KG for the financial support and the contribution to the completed and ongoing work.

References

1. N. Heinemann, J. Alcalde, J.M. Miocic, S.J.T. Hangx, J. Kallmeyer, C. Ostertag-Henning, A. Hassanpouryouzband, E.M. Thaysen, G.J. Strobel, C. Schmidt-Hattenberger, K. Edlmann, M. Wilkinson, M. Bentham, R.S. Haszeldine, R. Carbonell, A. Rudloff. Enabling large-scale hydrogen storage in porous media – the scientific challenges Energy Environ. Sci.,**14**, 853-864 (2021)
2. V. Nguyen, D.V. Papavassiliou, Hydrodynamic Dispersion in Porous Media and the Significance of Lagrangian Time and Space Scales. Fluids, **5**(2): 79 (2020)
3. D. Zivar, S. Kumar, J. Foroozesh, Underground hydrogen storage: A comprehensive review. International Journal of Hydrogen Energy 46(45), 23436-23462 (2021)
4. D.Y. Peng, D.B. Robinson, A New Two-Constant Equation of State. Industrial & Engineering Chemistry Fundamentals **15** (1), 59–64 (1976)
5. L.I. Stiel, G. Thodos, The viscosity of nonpolar gases at normal pressures, AIChE Journal **7** (4), 611–615 (1961)
6. J. Lohrenz, B. Bray, C. Clark, Calculating Viscosities of Reservoir Fluids From Their Compositions. Journal of Petroleum Technology **16** (10), 1171–1176 (1964)
7. J.T. Edward, Molecular volumes and the Stokes-Einstein equation, Journal of Chemical Education 47, 261 (1970)
8. M. R. Tek, *Underground Storage of Natural Gas*. Dordrecht: Springer Netherlands (1989)
9. T. K Perkins, O.C. Johnston, A Review of Diffusion and Dispersion in Porous Media, Society of Petroleum Engineers Journal **3** (01), 70–84 (1963):
10. A. Fick, Ueber diffusion. Annalen der Physik und Chemie **170**(1), 59–86 (1855).
11. E.N. Fuller, P.D. Schettler, J.C. Giddings, New method for prediction of binary gas-phase diffusion coefficients, Industrial & Engineering Chemistry **58**(5), 18–27 (1966)
12. E.N. Fuller, J.C. Giddings, A comparison of methods for predicting gaseous diffusion coefficients, Journal of Chromatographic Science **3**(7), 222–227 (1965)
13. E.N. Fuller, K. Ensley, J.C. Giddings, Diffusion of halogenated hydrocarbons in helium. the effect of structure on collision cross sections, The Journal of Physical Chemistry **73**(11), 3679–3685 (1969)
14. R.J Millington, J.P Quirk, Permeability of porous solids, Transactions of the Faraday Society **57**, 1200 (1961)
15. J. Bear, *Dynamics of Fluids in Porous Media*. Reprint. Originally published: New York: American Elsevier. Pub. Co., 1972. Originally published in series: Environmental science series (New York, 1972-), with corrections. New York: Dover Publ. (2013)
16. C.K. Ho, S.W. Webb, *Gas Transport in Porous Media*, Dordrecht: Springer Netherlands (SpringerLink Bücher, 20) (2006)
17. K. Soukup, P. Schneider, O. Šolcová, Comparison of Wicke–Kallenbach and Graham's diffusion cells for obtaining transport characteristics of porous solids, Chemical Engineering Science **63** (4), 1003–1011 (2008)

18. L.L. Chen, D.L. Katz, M.R. Tek, Binary gas diffusion of methane nitrogen through porous solids, AIChE Journal **23**(3), 336–341 (1977)
19. G. N. Pandey, M.R. Tek, D.L. Katz, Diffusion of Fluids Through Porous Media with Implications in Petroleum Geology. AAPG Bulletin **58** (1974)
20. G. Guevara-Carrion, S. Ancherbak, A. Mialdun, J. Vrabec, V. Shectsova, Diffusion of methane in supercritical carbon dioxide across the Widom line. Sci Rep **9**, 8466, (2019)
21. B. Strauch, P. Pilz, J. Hierold, M. Zimmer, Experimental simulations of hydrogen migration through potential storage rocks. International Journal of Hydrogen Energy (2023)
22. V. Arekhov, T. Zhainakov, T. Clemens, J. Wegner, Measurement of Effective Hydrogen-Hydrocarbon Gas Diffusion Coefficients in Reservoir Rocks, Paper SPE-214435-MS presented at the SPE EuropEC 2023, Vienna. Austria. 5-8 June 2023.
23. J.R. Taylor, W. Thompson. *An introduction to error analysis: the study of uncertainties in physical measurements*. Vol. 2. Mill Valley, CA: University science books, (1982)